Chemical Engineering Journal 102 (2004) 107–117

Chemical Engineering Journal

www.elsevier.com/locate/cej

Kinetic study of the combustion of methyl-ethyl ketone over α-hematite catalyst

G. Picasso Escobar, A. Quintilla Beroy, M.P. Pina Iritia*, J. Herguido Huerta

Department of Chemical and Environmental Engineering, University of Zaragoza, 50009 Zaragoza, Spain

Received 30 June 2003; accepted 19 September 2003

Abstract

The reaction kinetics of the catalytic combustion of methyl-ethyl ketone (MEK) in diluted air streams over Fe_2O_3 catalyst has been investigated in this work. The kinetic data base has been generated under quasi-differential conditions in a fixed bed reactor with Fe_2O_3 prepared by thermal decomposition and calcined at 600 °C. A series–parallel reaction network is proposed for the catalytic combustion of MEK, and several kinetic models have been tested, ranging from the simple power law model to mechanistic approaches. It has been found that the Langmuir–Hinshelwood mechanism with one type of active site over which adsorption of oxygen, MEK and carbon monoxide takes place, fits the experimental results obtained reasonably well. Moreover, the kinetic parameters so obtained are able to predict the performance of a Fe_2O_3 based catalytic membrane reactor.

Keywords: Catalytic combustion; Fe_2O_3; Kinetic modeling; Methyl-ethyl ketone; Catalytic membrane reactor

1. Introduction

Volatile organic compounds (VOC) constitute one important type of toxic pollutant responsible for photochemical smog leading to various environmental hazards. Increasing awareness over the last two decades has prompted the emergence of stricter regulations covering industrial activities. Catalytic combustion is one of the most promising alternatives for VOC removal from air streams [1–3], in particular when total destruction of a highly toxic compound present in low concentrations has to be ensured. In fact, this technology is well-developed by engineering companies because the operating costs are lower than for thermal combustion, and it is more flexible compared to other means of VOC elimination. When compared to thermal regenerative oxidation, catalytic oxidation with recuperative heat recovery may be economically advantageous for flow rates under 850 m^3 STP/min and VOC concentrations ranging from 50 to 10,000 ppmv [4].

In general, the performance of the catalytic combustion process depends on the type of catalyst, the reactor configuration and the nature of the VOC molecule. There are two main types of catalyst on the market [5] for the reduction of VOC emissions: supported noble metal catalysts [6–8] and metal oxides [9–18]; 75% [19] being precious metal based because these are generally supposed to be more active. The Catalytica study [5], however, compares the performance of both types, and the general conclusion is that metal oxides are not necessarily less active than noble metal catalysts. Moreover, noble metal catalysts are the most expensive. In the last few years, therefore, considerable efforts have been made to find more economical catalytic systems based on metal oxides. In this context, manganese based oxides such as MnO_2 [10], Mn_3O_4 [11], Mn_2O_3 [4], copper supported on alumina [12,14] and perovskite-type oxides [15–17] have, among others, been applied to VOC abatement processes. Of the publications found in the literature which address the use of Fe_2O_3 for VOC removal, most refer to its use as a noble metal catalyst support [20,21]. Scirè et al [22] compare the catalytic activity of the 1B metal (Au, Ag and Cu) supported on Fe_2O_3 in the oxidation of alcohols, and obtain a light-off temperature which, for the most active catalyst, is only 40 °C lower than that measured on Fe_2O_3. Bimetallic systems such as Fe_2O_3/ZrO_2 [23] have been used for NO abatement in the presence of hydrocarbons, Fe_2O_3 has been applied as a catalyst for methane combustion [24], and the employment of a catalytic membrane reactor with α-Fe_2O_3 as the active phase has also been tested [25]. Nevertheless, the formation of partially oxidised intermediates must be avoided, CO_2 and water being the only desired products. In this paper we report a study on the combustion of methyl-ethyl ketone (MEK), in excess oxygen over

* Corresponding author.
E-mail address: mapina@posta.unizar.es (M.P. Pina Iritia).

1385-8947/$ – see front matter © 2003 Elsevier B.V. All rights reserved.
doi:10.1016/j.cej.2003.09.006

α-hematite. The catalytic activity of different samples and the unwanted production of partially oxidised compounds, mainly CO, have been investigated to gain an insight into the performance of Fe_2O_3-based catalytic systems for VOC abatement processes. Among the solids prepared, the SI-2, denoted as the reference catalyst, has been used for the kinetic study. Several authors suggest that VOC oxidation on metal oxides occurs via the Mars-van Krevelen mechanism [11,22], implying lattice oxide ions as the active oxygen species; whereas others suggest that the adsorption of either the O_2 molecule or O atom is important [18]. In this paper, therefore, three kinetic models have been used to find which best fits the experimental data.

Apart from the above considerations, the catalytic systems used must operate under very demanding conditions: diluted streams, non-steady conditions, and high removal efficiency (usually higher than 95%). Finally, to be feasible the catalytic system should be able to handle high feed rates with a relatively low pressure drop, to ensure total VOC destruction at low temperatures and also to provide resistance to deactivation by fouling, poisoning or sintering. The combination of the above requirements represents a significant challenge in the present state of Chemical Reaction Engineering. One possible solution lies in the field of catalytic reactors based on porous membranes, currently offering very attractive research opportunities to academic and industrial scientists working on catalysis [26]. In our previous works, catalytic membrane reactors based on Pt/alumina [27,28], perovskites [29], or α-hematite [30]; operating in the Knudsen regime under flow-through configuration have demonstrated interesting performances [27,28] in the complete combustion of toluene, hexane or MEK. This type of gas–solid contactor, in which the permeation of a premixed feedstream takes place, provides an intimate contact between the molecules and the wall of the pores, thus minimising the diffusion resistance present in other systems such as fixed beds or monolith reactors. In particular, α-hematite based catalytic membranes [30], show a higher efficiency in the complete combustion of MEK than their bulk catalyst counterparts under equivalent experimental conditions. These results indicate that the membrane could perform very efficiently in the combustion of VOCs at low temperatures at the expense of a significant pressure drop. Its use would otherwise be restricted to applications involving reaction simultaneous with gas filtration, where a pressure drop is already present [31]. In such applications, the catalytic membrane reactor is capable of carrying out two operations at the same time: dust removal and catalytic abatement of VOCs.

The aims of the present work are: first, to explore the activity of Fe_2O_3-based catalysts for the oxidation of MEK, and secondly, to obtain a kinetic model to describe the catalytic combustion of the oxygenate, and apply the kinetics obtained to predict the experimental tendencies observed in an integral fixed bed reactor and a Fe_2O_3-based catalytic membrane reactor.

2. Experimental

2.1. Catalyst preparation and physicochemical characterisation

The starting materials used were $Fe(NO_3)_3{\cdot}9H_2O$ (Panreac, 98% pure) and NH_4OH solution (Panreac, 30% in NH_3, 28–30% pure). The catalysts were prepared by two different methods. The first, the *simple method*, consists of the filtration of a saturated nitrate solution in desionised water, followed by drying at 60 °C for 24 h and decomposition at 170 °C for 5 h to ensure NO_x removal ("SI" samples). For the catalysts prepared by the *precipitation method*, however, a NH_4OH solution is added to the $Fe(NO_3)_3$ saturated solution causing the precipitation of $Fe(OH)_3$. The mixing of the solution is carried out through a rapid addition of the ammonia solution ("RA" samples) or in a controlled way using 0.5 cm^3/min as NH_4OH addition rate ("CA" samples). As expected, a positive influence of low precipitation rates over the specific surface area was detected. The solids obtained were filtrated, dried and decomposed under the conditions described for the SI samples. Two different heating rates up to the calcination temperature were used: 2 and 10 °C/min. The SI samples were calcined at 600 °C for 6 h whereas for the catalysts prepared by precipitation, the calcination temperature was varied from 300 up to 600 °C in order to analyse its influence over the BET surface area, XRD spectra and light-off temperatures. Diffraction patterns were recorded using Cu Kα radiation with a step size of 0.010° and a step time of 2.5 s. The mean crystallite sizes were estimated using the Scherrer equation [33] and the selected reflection peaks (33°) were fitted by a Gaussian function. The sample prepared by the simple method calcined at 600 °C using 2 °C/min as heating rate, denoted as SI-2, has been adopted as the reference catalyst and used for the kinetic study due to the fact that a well-structured α-hematite phase is formed.

2.2. Reaction system

The catalytic combustion of MEK was performed in a 9 mm internal diameter tubular quartz reactor inside an electrical furnace operating at atmospheric pressure. The catalytic bed was 6 mm total length and 9 mm of diameter. The temperature was monitored by a thermocouple inserted in the centre of the catalyst bed in which 100 mg of catalyst diluted in 200 mg of glass dust, to avoid hot spots formation, was introduced and fixed over a trap. The experimental set up has been described in previous works [27–30].

The kinetic study was carried out in the tubular fixed bed reactor previously described using the operating conditions pointed out in the following Section 3.3 which ensures the reactor isothermicity due to lower conversions achieved (less than 30%).

The catalytic activity study was done from light-off curves showing the dependence of conversion (measured as MEK percentage consumed after the reaction) versus

reaction temperature. The typical combustion experiment began at 150 °C up to the temperature of total conversion, analyses being carried out every 15–20 °C. Temperatures $T_{50\%}$ and $T_{95\%}$ are defined as temperatures at which the conversion of MEK reaches values of 50% (light-off) and 95%, respectively.

Integral fixed bed reactor and catalytic membrane reactor experiments were carried out at two different space velocities, 70 and 170 h^{-1}, to assess the predictive capability of the kinetic model at higher levels of conversion. The catalytic membrane reactor operation and the membrane preparation procedure have already been described by Picasso et al. [30]. The permeation length of the membrane comprised the central 45 mm of the 90 mm long tube and the reaction temperature for the gas phase at the reactor inlet was measured by a thermocouple located axially in the membrane. The premixed MEK + air stream was fed to the internal side of the membrane and forced to permeate across to the γ-Al_2O_3 thin layer (5 μm thickness, 5 nm as nominal pore diameter) where the α-Fe_2O_3 was dispersed.

The exit gases from all reactors were analysed on-line by gas chromatography (HP 5890 model with FID detector) equipped with a methanation unit for CO and CO_2 determination. Carbon mass balance closures were always better than ±5%.

2.3. Data analysis

The kinetic reaction rate data were analysed with the commercial software Scientist, version 2.01 (Micromath Scientific Software). The Levenberg–Marquardt method was used to minimise the sum of squares of the deviations. The statistical parameters considered were the model selection criterion (MSC) and the determination coefficient (DC) for model comparison:

$$\mathrm{MSC} = \left(\frac{\sum_{i=1}^{n} (C_{\mathrm{obs},i} - \overline{C}_{\mathrm{obs},i})^2}{\sum_{i=1}^{n} (C_{\mathrm{obs},i} - C_{\mathrm{cal},i})^2} \right) - \frac{2p}{n} \quad (1)$$

$$\mathrm{DC} = \frac{\left[\sum_{i=1}^{n} (C_{\mathrm{obs},i} C_{\mathrm{cal},i}) - \left(\sum_{i=1}^{n} C_{\mathrm{obs},i} \sum_{i=1}^{n} C_{\mathrm{cal},i} \right) / n \right]^2}{\left[\sum_{i=1}^{n} (C_{\mathrm{obs},i})^2 - \left(\sum_{i=1}^{n} C_{\mathrm{obs},i} \right) / n \right] \times \left[\sum_{i=1}^{n} (C_{\mathrm{cal},i})^2 - \left(\sum_{i=1}^{n} C_{\mathrm{cal},i} \right) / n \right]} \quad (2)$$

where "p" refers to the number of parameters, "n" refers to the number of experimental data, and "C_{obs}" and "C_{cal}" are the exit MEK concentration (expressed in ppmv) observed experimentally and calculated with the model, respectively.

2.4. Reactor simulation

The integral fixed bed reactor and catalytic membrane reactor were simulated by an engineering model developed in Fortran 77. The main assumptions made in order to derive the model equations are isothermal conditions, and the gas being in plug flow and behaving ideally. The flow domain is considered as one dimensional. The material balance equations for MEK, CO and CO_2 are discretized according to the volume element formulation and solved using a 4th order Runge–Kutta based method. The kinetic model and experimental data published by van de Beld et al. [33] for catalytic oxidation of 2750 ppmv of ethene in air over Pd/Al_2O_3 in a packed bed reactor were used to validate the reactor simulation program. The comparison of the experimental data and that predicted by the model is shown in Fig. 1.

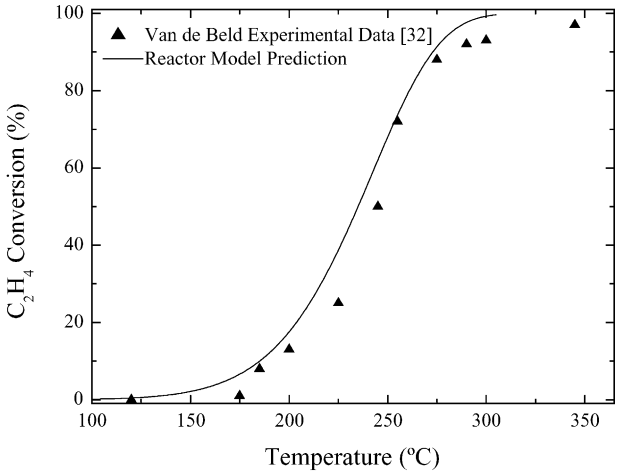

Fig. 1. Comparison of ethylene experimental light-off curve with the profile calculated from the use of published kinetic parameters [32] and the developed reactor model. Experimental conditions: $(C_2H_4)_0 = 2750$ ppmv; $u_{g,0} = 0.26$ m/s; $L = 0.20$ m; 0.41 wt.% Pd/Al_2O_3.

3. Results and discussion

3.1. Fe_2O_3 bulk catalyst characterisation

The main properties of the catalytic samples studied in this work are summarised in Table 1. The XRD spectra used for crystallite diameter estimations are compiled in Fig. 2. All diffractograms correspond to the α-hematite crystallographic phase of Fe_2O_3 with the exception of

Table 1
Main properties of the bulk catalysts tested in this work

Catalyst sample	Heating rate (°C/min)[a]	$T_{calcination}$ (°C)	BET area (m^2/g catalyst)	$D_{crystallite}$ (nm)
SI-1	–	Uncalcined	55.7	14
SI-2	2	600	5.5	30
RA-1	–	Uncalcined	26.4	–
RA-2	2	300	22.4	19
RA-3	2	400	20.2	19
RA-4	2	500	12.9	21
RA-5	2	600	6.5	26
CA-1	–	Uncalcined	41.2	–
CA-2	2	300	39.9	20
CA-3	10	300	57.0	16
CA-4	2	600	1.3	30
CA-5	10	600	3.1	29

[a] Heating rate used up to the calcination temperature.

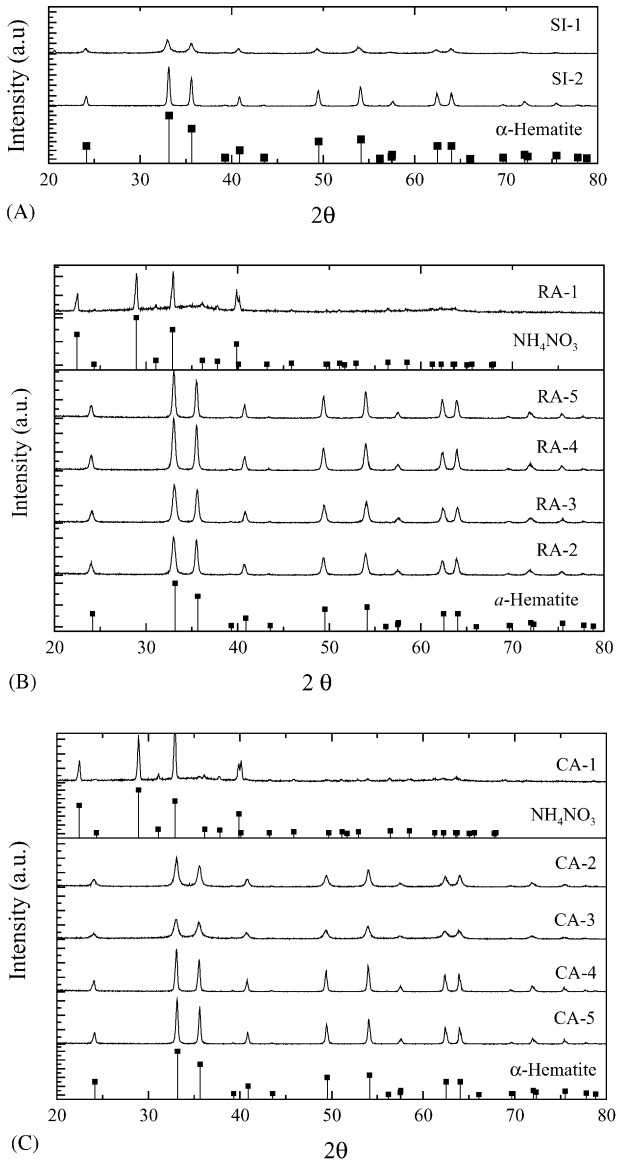

Fig. 2. XRD spectra of the bulk catalysts prepared: (A) SI samples; (B) RA samples; (C) CA samples.

the uncalcined samples RA-1 and CA-1, prepared by the precipitation method, where the characteristic diffraction peaks of ammonium nitrate are observed, probably covering the surface of Fe_2O_3 crystallites. This is due to the fact that the decomposition temperature of NH_4NO_3 (180 °C) is higher than that corresponding to $Fe(NO_3)_3$ (170 °C). Nevertheless, it is important to emphasise that the reaction temperatures are always higher than these values, therefore the α-hematite could be expected as active phase.

A BET surface area loss caused by calcination is observed, less pronounced in the case of the RA samples which gave the lowest values reported for calcination temperatures of less than 600 °C. The slow addition of the base, used in the preparation of the "CA" samples, provokes a controlled precipitation of the hydroxide and renders a higher specific area

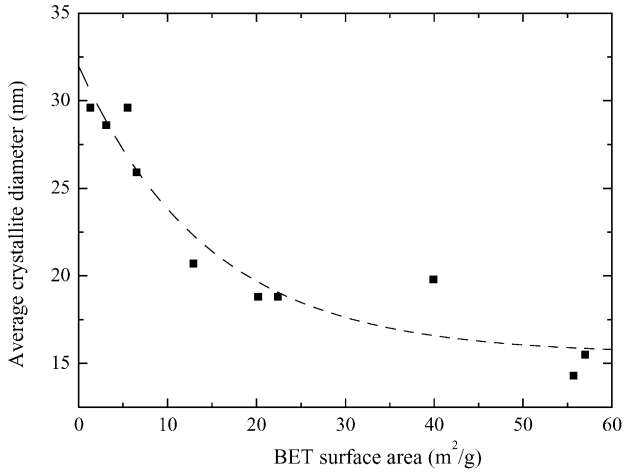

Fig. 3. Relationship between average crystallite diameter and BET surface area for the α-hematite catalysts prepared.

of the calcined solids with respect to their "RA" counterparts (39.9 m^2/g for CA-2 versus 22.4 m^2/g for RA-2). A similar effect is observed when high heating rates up to the calcination temperatures are used (57.0 m^2/g for CA-3 versus 39.9 m^2/g for CA-2); probably due to the solids formed being unable to accommodate to the temperature profile imposed, and therefore, particle agglomeration is partially avoided. Moreover, a good correlation between BET surface area and average crystallite diameter has been found (see Fig. 3).

3.2. Catalytic activity of Fe_2O_3 bulk catalysts

The Fe_2O_3 bulk catalysts were tested for total combustion of MEK in order to measure their activity and to evaluate the influence of three different factors over the performance of the catalytic system: weight hourly space velocity, feed concentration and preparation method. Previously, some blank experiments were carried out with fine quartz, demonstrating the absence of activity up to 400 °C. Table 2 compiles the

Table 2
Catalytic activity in MEK combustion[a] of selected samples

Catalyst sample	BET area (m^2/g catalyst)	$T_{50\%}$ (°C)	$T_{95\%}$(°C)	$T_{max,CO}$ (°C)
SI-1	55.7	250	286	250
SI-2	5.5	285	326	285
RA-1[b]	26.4	238	266	240
RA-2	22.4	266	299	267
RA-3	20.2	–	–	–
RA-4	12.9	–	–	–
RA-5[b]	6.5	282	316	285
CA-1	41.2	271	297	270
CA-2	39.9	282	322	280
CA-3	57.0	259	288	260
CA-4	1.3	323	370	315
CA-5	3.1	309	350	310

[a] $[MEK]_0 = 1900$ ppmv, WHSV $= 80\ h^{-1}$.
[b] $[MEK]_0 = 1500$ ppmv.

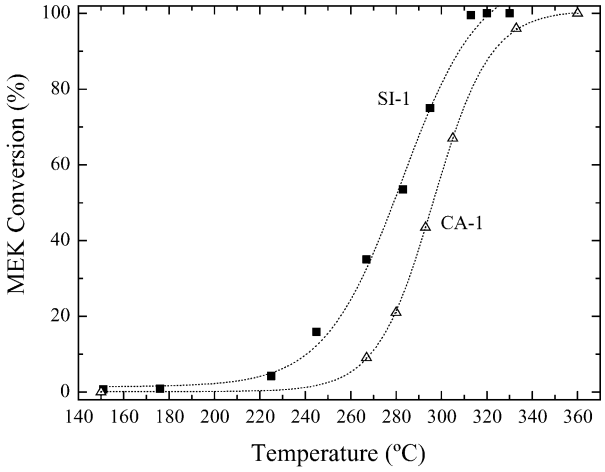

Fig. 4. Effect of preparation method over catalytic performance: SI-1 and CA-1 samples. Experimental conditions: $(MEK)_0 = 2000$ ppmv; WHSV $= 170\,h^{-1}$. *Note*: Temperatures reported have been measured inside the catalytic bed.

$T_{50\%}$ and $T_{95\%}$ values and also the temperatures at which the exit CO concentration is at a maximum, for given reaction conditions (1900 ppmv of MEK and $80\,h^{-1}$ as WHSV). An analysis of the calcination influence over the catalytic performance reveals that calcined samples at low heating rates (i.e. 2 °C/min) exhibit higher light-off temperatures due to the loss of BET surface area by particle sintering. The preparation method has also been analysed in terms of catalytic performance. When comparing the SI-2, RA-5 and CA-4 samples (calcined at 600 °C) with the SI-1, RA-1 and CA-1 (uncalcined), differences in $T_{50\%}$ values varying from 35 to 52 °C are observed. A less pronounced tendency is found when the heating rate factor is studied. The experimental results indicate that controlled addition samples are less active than simple impregnation ones, as is illustrated in Fig. 4 where the CA-1 and SI-1 light-off curves are compared. A similar trend is obtained for the CA-4 and SI-2 samples (see Table 2) where a total conversion temperature difference of 44 °C is detected. When this procedure was applied to catalytic membrane preparation [30], a different behaviour was observed. For supported α-hematite catalysts, the hydroxide precipitation inside the porous structure of the support membrane allows the confinement of the catalytic material within an area in which Knudsen diffusion for reactants is ensured, and therefore enhanced conversions were achieved.

All the samples tested yield total combustion products when total conversion of MEK is reached (see Table 2). However, the CO concentration presents a maximum at the light-off temperature according to a series reaction network: CO formation from MEK and CO depletion to CO_2. The influence of space velocity on light-off curves and total combustion performance is shown in Fig. 5A and B. The $T_{50\%}$ increases with the total feed flow rate from 238 °C at $80\,h^{-1}$ to about 278 °C at $170\,h^{-1}$; whereas the maximum selectivity to CO decreases. Therefore, the yield to CO shifts to

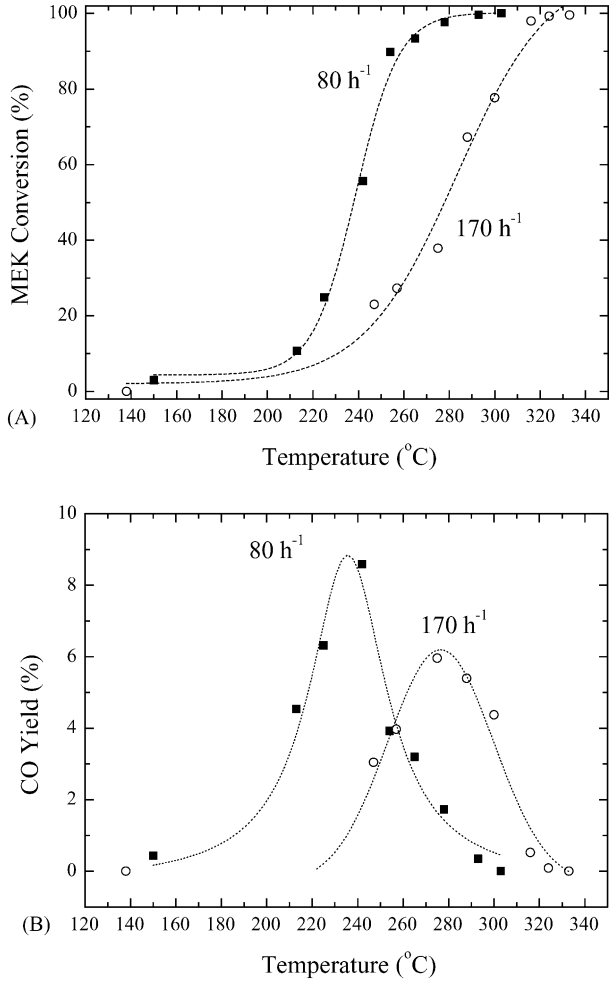

Fig. 5. Effect of weight hourly space velocity over RA-1 sample: (A) light-off curves; (B) yield to CO. Experimental condition: $(MEK)_0 = 1550$ ppmv. *Note*: Temperatures reported have been measured inside the catalytic bed.

lower values when the total flow rate increases (from 8.8 to 6.3%, respectively).

The experiments carried out over the SI-2 sample at different feed concentrations, shown in Fig. 6A (480 and 1700 ppmv), are in agreement with a pseudo-reaction total order "*n*" with respect to the oxygenate within the range $1 > n \geq 0$, i.e. light-off temperatures increase with MEK concentration (from 265 to 291 °C). However, the yield to CO at MEK isoconversion slightly increases with the MEK concentration, probably because it is associated with a reaction order with respect to the oxygenate higher for the CO formation than for the CO_2 production. Fig. 6B shows the evolution of yield to CO versus reaction temperature. As can be observed, this shifts from 4.8 to 5.8% when the MEK concentration increases from 480 to 1700 ppmv.

3.3. Kinetic modelling

The range of operating conditions for the kinetic study was as follows: catalyst SI-2, constant temperature measured

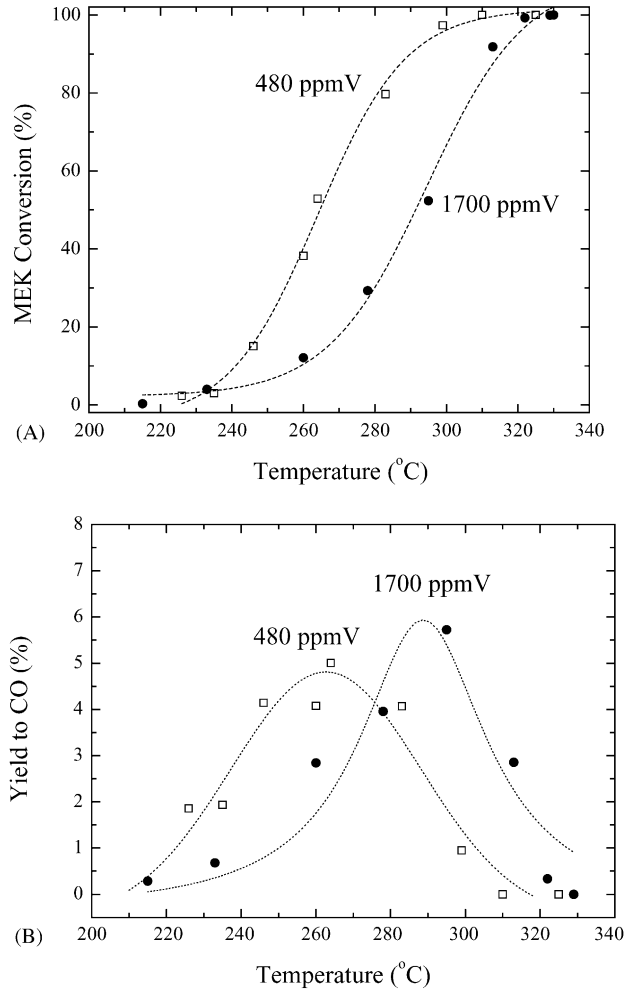

Fig. 6. Effect of MEK concentration over SI-2 sample: (A) light-off curves; (B) yield to CO. Experimental condition: WHSV = 75 h^{-1}. *Note*: Temperatures reported have been measured inside the catalytic bed.

inside the catalytic bed, 250–305 °C; MEK concentration in the air stream, 500–2000 ppmv and weight hourly space velocity defined per total feed flow rate, 70–500 h^{-1}. In all these experiments, the MEK conversion level was less than 30%. The particle size of the catalyst was chosen in order to minimise internal mass transfer resistance (160–320 μm). Previous reaction experiments using different total flow rates and maintaining the space velocity and MEK concentration constant confirmed the absence of external mass transfer limitations at flow rates above 100 cm^3 STP/min, the lowest limit used in the experiments.

The experimental points corresponding to the data plotted in Figs. 8 and 9, generated in the differential reactor under isothermal conditions with the SI-2 catalyst were fitted with both an empirical power-law model and mechanistic models. As a first approximation to the reaction kinetics, and for model discrimination purposes, the total MEK depletion rate was considered. However, once the best model was identified, the kinetics corresponding to the series–parallel reaction network shown in Fig. 7 was studied.

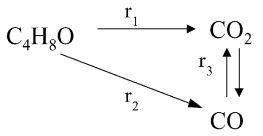

Fig. 7. The series–parallel reaction scheme adopted for MEK combustion.

3.4. Power law model

Modelling data with power law expressions help to quantify the effect of the principal variables—temperature and reactant partial pressures—on the reaction rates. The MEK consumption rate was fitted to the following equation:

$$-r_{\mathrm{MEK}} = \frac{-\mathrm{d}C_{\mathrm{MEK}}}{\mathrm{d}t} = kC_{\mathrm{MEK}}^{n}C_{\mathrm{O_2}}^{m} \tag{3}$$

where r_{MEK} is the MEK reaction rate (ppmv/h), and C_{MEK} and CO_2 are respectively the MEK and O_2 concentrations at the reactor outlet (ppmv). Because a clear excess of air has been employed in all the experiments, the oxygen concentration can be considered nearly constant throughout the reactor, and therefore the reaction rate can be expressed as follows:

$$-r_{\mathrm{MEK}} = \frac{-\mathrm{d}C_{\mathrm{MEK}}}{\mathrm{d}t} = k'C_{\mathrm{MEK}}^{n} \tag{4}$$

The resulting apparent kinetic constant k' was fitted to the Arrhenius equation:

$$k' = k'_0 \exp\left(-\frac{E_{\mathrm{a}}}{R}\left(\frac{1}{T} - \frac{1}{T_{\mathrm{m}}}\right)\right) \tag{5}$$

where T_{m} is a reference temperature (473.15 K) and k'_0 the kinetic constant at that temperature.

This empirical model fits the data well with a reasonably high value of 3.57 for the MSC. The activation energy estimated, 117 kJ/mol, is similar to the reported value [4] for MEK combustion over Mn_2O_3, 118 kJ/mol. The reaction order with respect to MEK was estimated at 0.36, in agreement with the light-off temperature—oxygenate concentration dependency, as was shown in Fig. 6. Such reaction order clearly was pointing at more detailed mechanisms, such as those explained in the following section.

The values of the kinetic parameters for the MEK depletion rate, the DC and the MSC parameters for all the kinetic models tested, including the mechanistics ones, are shown in Table 3.

3.5. Mechanistic approaches: Mars-van Krevelen and Langmuir–Hinshelwood models

Mechanistic models are supposed to decouple the chemical reaction into elementary reaction steps, providing an insight into how effectively to optimise the catalyst performance and reactor configuration. Two basic mechanistic models were tested: Mars-van Krevelen and Langmuir–Hinshelwood. In the former one, a coupled redox

Table 3
Estimated kinetic parameters[a] for total MEK depletion rate of the different models tested.

Kinetic parameters	MEK + α-O_2 → reaction products (CO, CO_2, H_2O)		
	Power-law	Mars-van Krevelen	Langmuir–Hinshelwood
n	0.36	1	1
MSC	3.5691	3.6064	3.6540
DC	0.9733	0.9748	0.9760
k' (ppmv/h)	46.2		
E_a (kJ/mol)	117	131, 96.2	102, −25.7
k_{MVK} (ppmv/h)		524.8	
k_i (ppmv/h)		3.7	
k_{LH} (ppmv/h)			2.3
k'_{LH} (ppmv/h)			1.3×10^{-3}

[a] All the kinetic constants tabulated have been evaluated at 473 K.

process between oxygen, active sites and MEK takes place. Oxygen reacts with a reduced catalytic site and the VOC molecule subsequently reacts with the oxidised centre, and therefore gas phase oxygen regenerates the catalyst lattice. The elementary steps involved are:

$$O_2 + Z \xrightarrow{k_{0i}} Z_o \tag{6}$$

$$MEK + Z_o \xrightarrow{k_i} \text{products} + Z \tag{7}$$

The corresponding MEK and O_2 reaction rates are defined as

$$-r_{MEK} = \frac{-dC_{MEK}}{dt} = k_i C_{MEK}\theta \tag{8}$$

$$-r_{O_2} = \frac{-dC_{O_2}}{dt} = k_{0i} C_{O_2}(1-\theta) \tag{9}$$

where θ refers to the fraction of oxidised activated centres "Z_o" and $(1-\theta)$ to the reduced centres "Z". Defining "α" as the number of oxygen moles which disappear per mole of MEK, and combining Eqs. (8) and (9), the following expression is obtained:

$$\frac{1}{-r_{MEK}} = \frac{\alpha}{k_{0i}C_{O_2}} + \frac{1}{k_i C_{MEK}} = \frac{1}{k_{MVK}} + \frac{1}{k_i C_{MEK}} \tag{10}$$

As is observed in Table 3, the apparent activation energies are similar to that estimated previously, 131.1 and 96.2 kJ/mol for k_{MVK} and k_i, respectively. A mechanistic model including the adsorption of the reactants as elementary steps has also been tested. The Langmuir–Hinshelwood approach is essentially a one site model, i.e. both reactants adsorb onto the surface and the reaction takes place between the adsorbed species. This type of mechanism has already been reported in the literature [18] for MEK oxidation over Mn_2O_3 catalysts. In the present work, dissociative O_2 adsorption is postulated; however, several modifications could be developed considering specific active adsorption sites for each reactant or product. The set of elementary reaction steps considered are the following:

$$MEK + {}^{\bullet} \overset{K_i}{\leftrightarrow} MEK^{\bullet}; \quad K_i = \frac{[MEK^{\bullet}]}{[MEK][^{\bullet}]} \tag{11}$$

$$O_2 + 2^{\bullet} \overset{K_{0i}}{\leftrightarrow} 2O^{\bullet}; \quad K_{0i} = \frac{[O^{\bullet}]^2}{[O_2][^{\bullet}]^2} \tag{12}$$

$$MEK^{\bullet} + O^{\bullet} \xrightarrow{k} \text{products}; \quad -r_{MEK} = k\,[MEK^{\bullet}]\,[O^{\bullet}] \tag{13}$$

where $[^{\bullet}]$ represents the fraction of free active sites over the catalyst surface. Applying the balance equation to the active centres, assuming that O_2 concentration remains constant due to the clear excess used and rearranging (11) and (12), the following kinetic equation is obtained:

$$-r_{MEK} = \frac{kK_i C_{MEK}\sqrt{K_{0i}C_{O_2}}}{\left(1+\sqrt{K_{0i}C_{O_2}}+K_i C_{MEK}\right)^2} \tag{14}$$

If $(K_{0i}C_{O_2})^{1/2}$ is negligible, the MEK depletion rate could be expressed as follows:

$$-r_{MEK} \approx \frac{k_{LH}C_{MEK}}{(1+k'_{LH}\cdot C_{MEK})^2};$$
$$k_{LH} = kK_i\sqrt{K_{0i}C_{O_2}}; \quad k'_{LH} = K_i \tag{15}$$

Fig. 8 shows the parity MEK concentration plots at the reactor exit for the three models. Although no significant differences are observed in the model selection criteria values when the three models are compared, the Langmuir–Hinshelwood approach renders the highest value of MSC (3.654). For this reason, and due to the experimentally observed relationship between specific surface area of the catalytic samples and light-off temperatures, this model has been selected to gain an insight into the kinetics of the series–parallel reaction network shown in Fig. 7.

3.6. Langmuir–Hinshelwood model for the series–parallel reaction network

In the reaction scheme adopted to describe the MEK oxidation process, the reaction rates involved are:

$$R_1 = \frac{-dC_{MEK\to CO_2}}{dt}; \qquad R_2 = \frac{-dC_{MEK\to CO}}{dt};$$
$$R_3 = \frac{-dC_{CO\to CO_2}}{dt} \tag{16}$$

Three different LH models have been developed, each of which considers that MEK reacts to give CO and CO_2, that there is only one type of adsorption site whatever the nature of the species, that product desorption is not controlling the reaction rate, and also that there is a new elementary reaction step in which the intermediate molecule CO is implicated. In the first model, LH-1, there is no adsorption of CO but the active sites over which atomic oxygen is adsorbed interact with CO to produce CO_2 which can be further decomposed to CO. The second model, LH-2, considers a reversible homogeneous reaction in gas phase between carbon monoxide and oxygen. And finally, the LH-3 model assumes

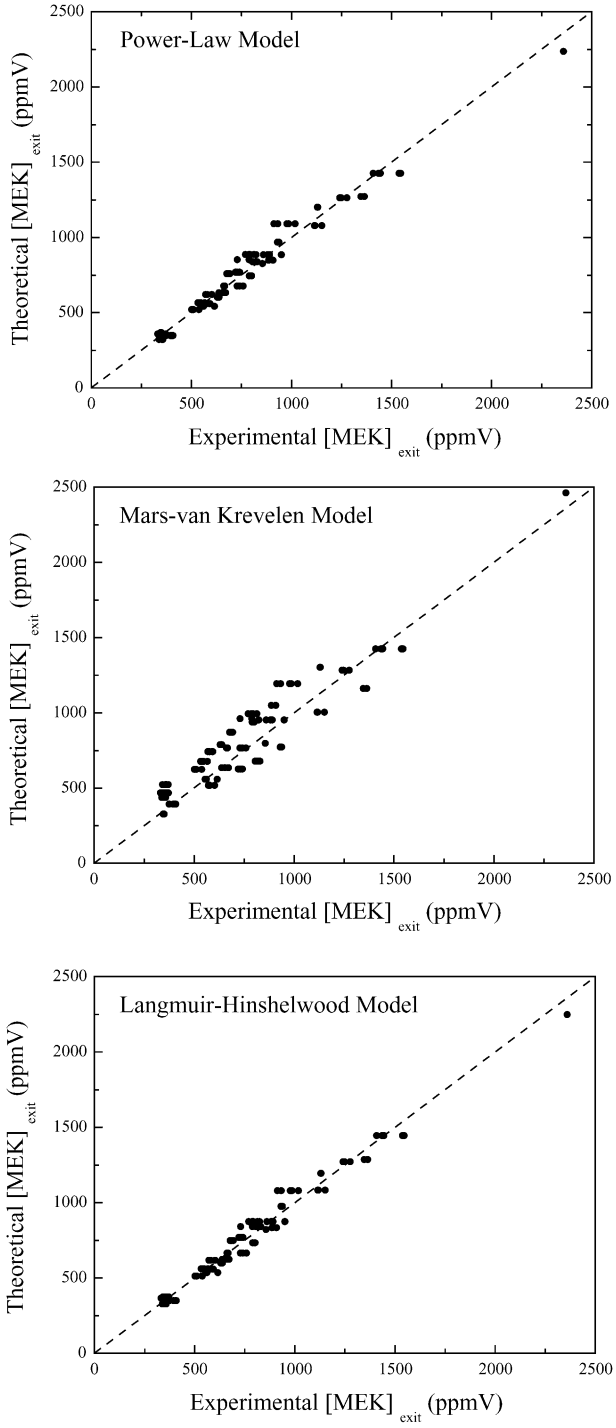

Fig. 8. Parity plots for MEK concentration at the reactor outlet for the different models tested.

that CO and O_2 previously adsorbed react to CO_2 which can also be decomposed to CO. The statistical parameters improve from model LH1 (MSC = 4.4964, DC = 0.9898) to model LH-2 (MSC = 4.5462, DC = 0.9903) and LH-3 (MSC = 4.5796, DC = 0.9908). There is a substantial increase in the MSC compared to that calculated previously, indicating that the complex reaction scheme adopted appropriately represents the oxidation process. The elementary reaction steps and reaction rate expressions for the best fit, mechanism LH-3, have been summarised in Table 4. The estimated kinetic parameters for this mechanism are collected in Table 5, while the comparison between the experimental MEK and CO concentrations at the reactor outlet and the predicted values is shown in Fig. 9A and B, respectively. It should be emphasised that k' and k'' are artificial kinetic constants resulting from an algebraic combination, therefore negative activation energies can be achieved. Moreover, the kinetic constants for CO_2 (k_1) and CO (k_2) formation from MEK are quite similar, although the activation energy for the former is notably higher (114.4 kJ/mol versus 77.2 kJ/mol), in agreement with the CO_2 selectivity increase with temperature above the $T_{50\%}$ value. Under these conditions, the temperature effect on the reaction rate is more noticeable

Table 4
Elementary reaction steps and reaction rate expressions for LH-3 model

Adsorption elementary steps: equilibrium assumption	
$MEK + {}^{\bullet} \overset{K_1}{\leftrightarrow} MEK^{\bullet}$	$K_1 = \dfrac{[MEK^{\bullet}]}{[MEK][{}^{\bullet}]}$
$O_2 + 2{}^{\bullet} \overset{K_2}{\leftrightarrow} 2O^{\bullet}$	$K_2 = \dfrac{[O^{\bullet}]^2}{[O_2][{}^{\bullet}]^2}$
$CO + {}^{\bullet} \overset{K_3}{\leftrightarrow} CO^{\bullet}$	$K_3 = \dfrac{[CO^{\bullet}]}{[CO][{}^{\bullet}]}$
Reaction elementary steps: reaction rate expressions	
$MEK^{\bullet} + O^{\bullet} \overset{k_A}{\rightarrow} 4CO_2$	$R_1 = \dfrac{k_1 C_{MEK}}{(1 + k' C_{MEK} + k'' \cdot C_{CO})^2}$
	$k_1 = \dfrac{k_A K_1 \sqrt{K_2 C_{O_2}}}{(1 + \sqrt{K_2 O_2})^2}$
	$k' = \dfrac{K_1}{(1 + \sqrt{K_2 O_2})}$; $k'' = \dfrac{K_3}{(1 + \sqrt{K_2 O_2})}$
$MEK^{\bullet} + O^{\bullet} \overset{k_B}{\rightarrow} 4CO$	$R_2 = \dfrac{k_2 C_{MEK}}{(1 + k' C_{MEK} + k'' C_{CO})^2}$
	$k_2 = \dfrac{k_B K_1 \sqrt{K_2 C_{O_2}}}{(1 + \sqrt{K_2 O_2})^2}$
	$k' = \dfrac{K_1}{(1 + \sqrt{K_2 O_2})}$; $k'' = \dfrac{K_3}{(1 + \sqrt{K_2 O_2})}$
$CO^{\bullet} + O^{\bullet} \overset{k_C}{\rightarrow} CO_2 + 2O^{\bullet}$	$R_3 = \dfrac{k_3 C_{CO}}{(1 + k' C_{MEK} + k'' C_{CO})^2} - k'_3 C_{CO_2}$
$CO_2 \overset{k'_C}{\rightarrow} CO + \frac{1}{2}O_2$	$k_3 = \dfrac{k_C K_3 \sqrt{K_2 C_{O_2}}}{(1 + \sqrt{K_2 O_2})^2}$; $k'_3 = k'_C$
	$k' = \dfrac{K_1}{(1 + \sqrt{K_2 O_2})}$; $k'' = \dfrac{K_3}{(1 + \sqrt{K_2 O_2})}$

Table 5
Estimated kinetic parameters for LH-3 model

Kinetic constants[a] (ppmv/h)		Activation energies (kJ/mol)	
k_1	1.5	E_{a_1}	114.4
k_2	1.3	E_{a_2}	77.2
k_3	187.8	E_{a_3}	32.0
k'_3	23.3	E'_{a_3}	4.5×10^{-1}
k'	4.7×10^{-4}	E'_a	1.7
k''	6.1×10^{-2}	E''_a	−90.9

[a] All the kinetic constants tabulated have been evaluated at 473 K.

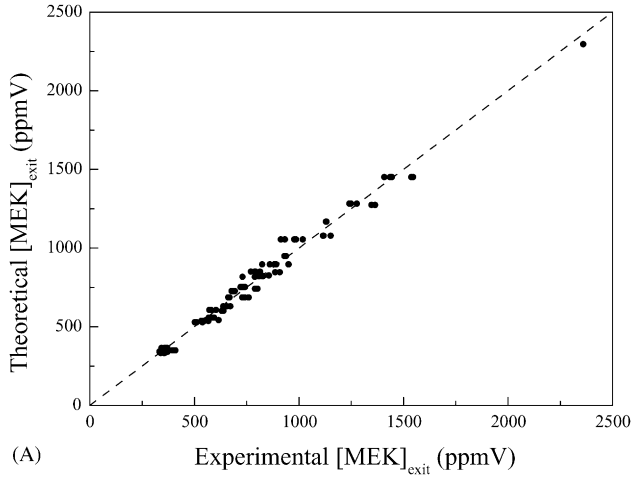

Fig. 9. Parity plots for: (A) MEK; (B) CO concentration at the reactor outlet for LH-3 model.

than the concentration dependency. However, the estimated kinetic parameters are not able to predict the CO concentration with sufficient accuracy, probably due to the relatively low experimental values detected and the intrinsic error in their analytical measurement.

3.7. Integral fixed bed reactor simulation with LH-3 model

In order to check the suitability of the LH-3 kinetic model, we simulated the light-off curves obtained with a catalytic fixed bed reactor operating under integral conditions. Fig. 10A–C illustrate the goodness of the fitting evaluated for the reference catalyst and RA-5 catalyst under specific reaction conditions. The Langmuir–Hinshelwood model overpredicts the selectivity to CO although it is capable of reproducing the changes in yield to CO with temperature.

3.8. Catalytic membrane reactor simulation with LH-3 model

We have also simulated the light-off curves obtained with a Fe_2O_3 catalytic membrane reactor in which the MEK con-

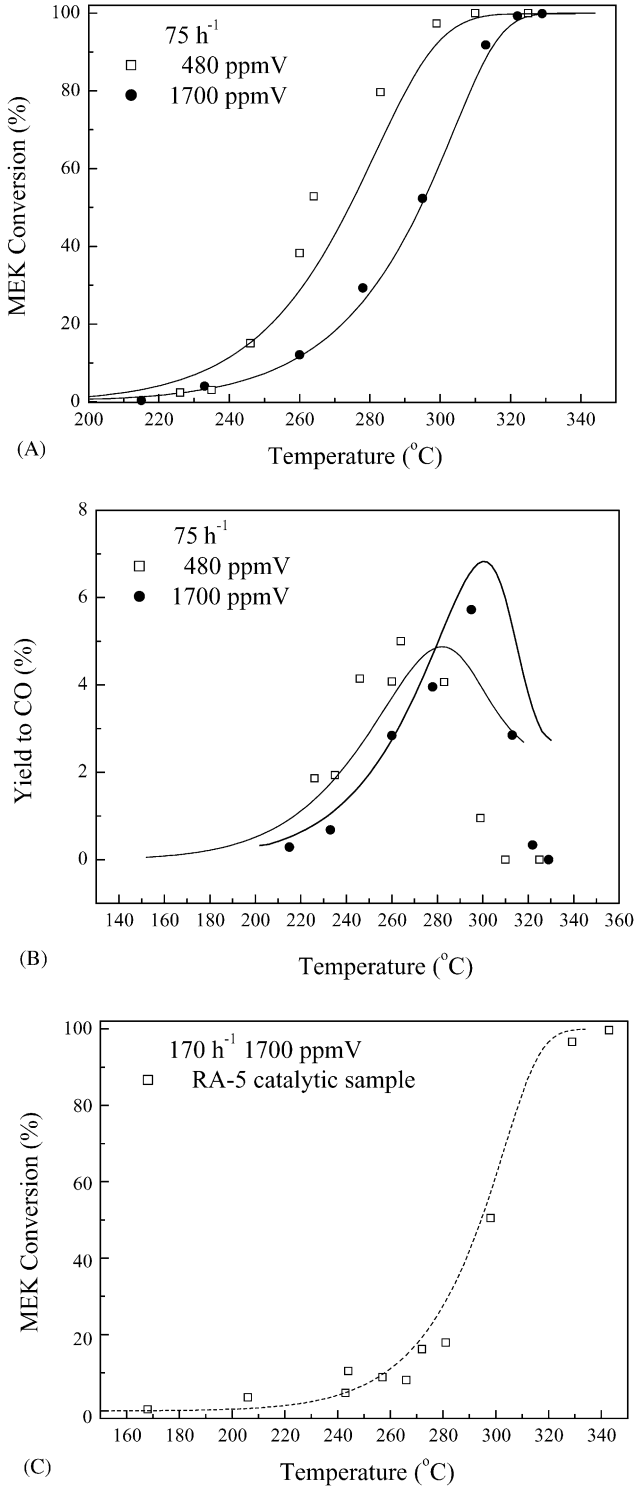

Fig. 10. Simulation of an integral fixed bed reactor using the LH-3 kinetic model: (A) light-off curves; (B) yield to CO for SI-2 catalyst, 75 h^{-1}, 480 ppmv and 1700 ppmv MEK, respectively; (C) light-off curve for RA-5 catalyst, 170 h^{-1} and 1700 ppmv MEK. *Note*: Temperatures reported have been measured inside the catalytic bed.

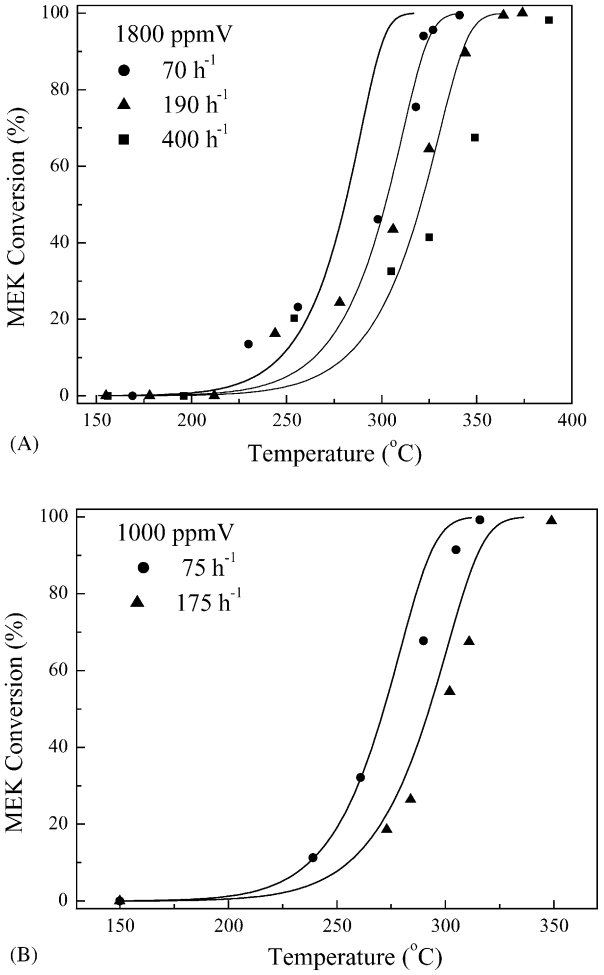

Fig. 11. Simulation of the light-off curves obtained with a Fe_2O_3 based catalytic membrane reactor: (A) 1800 ppmv MEK; (B) 1000 ppmv MEK. Symbols: experimental points; lines: predicted values. *Note*: Temperatures reported have been measured in the gas phase at the reactor inlet.

centration varied significantly across the membrane wall. A comparison of experimental and simulated data is shown in Fig. 11A and B for an stainless steel catalytic membrane prepared under similar conditions to those employed with SI-2. As is observed, the experimental tendencies are predicted reasonably well, assuming the hypothesis for the reactor modelling already quoted. However, the simulated curves are always shifted to lower temperatures indicating a gas–solid contact efficiency higher than the achieved experimentally. This is probably due to part of the active material deposited onto the membrane is located in a dead-end pore or inaccessible area, and therefore does not participate in the reaction.

4. Conclusions

Several kinetic models were tested to characterise the oxidation of MEK over α-hematite catalysts. For a series–parallel reaction scheme which best describes the process, a Langmuir–Hinshelwood model appears as the more realistic approach which fits the experimental results obtained reasonable well.

This model assumes that the catalyst has only one type of active site over which MEK, oxygen and carbon monoxide are adsorbed. The kinetics so obtained was successfully applied to simulate the light-off curves of MEK and the product distribution obtained in an integral catalytic fixed bed reactor. Moreover, this model, which considers isothermal behaviour, gas in plug flow and negligible radial concentration gradients, is able to predict reasonably well the performance of a Fe_2O_3 catalytic membrane reactor in the MEK oxidation process.

References

[1] J. Spivey, Ind. Eng. Chem. Res. 26 (1987) 2165–2180.
[2] E. Moretti, N. Mukhopadhyay, Chem. Eng. Prog. 89 (7) (1993) 20–26.
[3] F.I. Khan, A.Kr. Ghoshal, J. Loss Prev. Proc. Ind. 13 (2000) 527–545.
[4] L.M. Gandía, A. Gil, S.A. Korili, Appl. Catal. B: Environ. 33 (2001) 1–8.
[5] J.A. Horshley, Catalytica Environmental Report E4, Catalytica Studies Division, Mountain View, CA, USA, 1993.
[6] E.M. Cordi, J.L. Falconer, J. Catal. 162 (1) (1996) 104–117.
[7] N. Burgos, M. Paulis, M. Antxustegui, M. Montes, Appl. Catal. B: Environ. 38 (2002) 251–258.
[8] M.A. Centeno, M. Paulis, M. Montes, J.A. Odriozola, Appl. Catal. A: Gen. 234 (2002) 65–78.
[9] J.L. Falconer, E.M. Cordi, P.J. O'Neill, Appl. Catal. B: Environ. 14 (1-2) (1997) 23–36.
[10] C. Lahousse, A. Bernier, P. Grange, B. Delmon, P. Papaefthimiou, T. Ioannides, X. Verkyos, J. Catal. 178 (1998) 214–225.
[11] M. Baldi, E. Finocchio, F. Milella, G.A. Busca, Appl. Catal. B: Environ. 16 (1998) 43–51.
[12] N. Ali, C. Lu, R. Masel, Catal. Today 62 (2000) 347–353.
[13] H-G. Lintz, K. Wittstock, Appl. Catal. A: Gen. 216 (2001) 217–225.
[14] S.C. Kim, J. Haz. Mater. B91 (2002) 285–299.
[15] S. Irusta, M.P. Pina, M. Menéndez, J. Santamaría, J. Catal. 179 (2) (1998) 400–412.
[16] K. Poplawski, J. Lichtenberger, F.J. Keil, K. Schnitzlein, M.D. Amiridis, Catal. Today 62 (2000) 329–336.
[17] V. Blasin-Aubé, J. Belkouch, L. Moceaux, Appl. Catal. B: Environ. 43 (2) (2003) 175–186.
[18] T.K. Tseng, H. Chu, Sci. Tot. Environ. 275 (2001) 83–93.
[19] R.K. Sharma, B. Zhou, S. Tong, K.T. Chuang, Ind. Eng. Chem. Res. 34 (1995) 4310–4317.
[20] M. Haruta, A. Ueda, S. Tsubota, R.M.T. Sanchez, Catal. Today 29 (1–4) (1996) 443–447.
[21] U. Rodemerck, D. Wolf, O.V. Buyevskaya, P. Claus, S. Senkan, M. Baerns, Chem. Eng. J. 82 (1–3) (2001) 3–11.
[22] S. Scirè, S. Minicò, C. Crisafulli, S. Galvagno, Catal. Commun. 2 (2001) 229–232.
[23] S. Tuti, F. Pepe, D. Pietrogiacomi, V. Indovina, Catal. Today 75 (1–4) (2002) 373–378.
[24] A. Sanz, A.L. Barbosa, A. Monzón, J. Herguido, J. Santamaría, Stud. Surf. Sci. Catal. 139 (2001) 487–494.
[25] M. González-Burillo, A.L. Barbosa, J. Herguido, J. Santamaría, J. Catal. 258 (2003) 457–459.
[26] J. Coronas, J. Santamaría, Catal. Today 51 (1999) 377–389.
[27] M.P. Pina, M. Menéndez, J. Santamaría, Appl. Catal. B 11 (1996) 19–27.
[28] M.P. Pina, S. Irusta, M. Menéndez, J. Santamaría, R. Hughes, N. Boag, Ind. Eng. Chem. Res. 36 (1997) 4557–4566.

[29] S. Irusta, M.P. Pina, M. Menéndez, J. Santamaría, Catal. Lett. 54 (1998) 69–78.
[30] G. Picasso, A. Quintilla, M.P. Pina, J. Herguido, Appl. Catal. B: Environ. 46 (2003) 133–143.
[31] G. Saracco, V. Specchia, Chem. Eng. Sci. 55 (2000) 897–908.
[32] L. Van de Beld, M.P.G. Bijl, A. Reinders, B. Van der Werf, K.R. Westerterp, Chem. Eng. Sci. 49 (24A) (1994) 4361–4373.
[33] B.D. Cullity, Elements of X-ray Diffraction, first ed., Addison-Wesley, Reading, MA, 1959, p. 132.